Interaction-Aware Traffic Prediction and Scenario-Based Model Predictive Control for Autonomous Vehicles on Highways

Xiaorong Zhang, Sahar Zeinali, and Georg Schildbach

***Abstract*— This article addresses the problem of traffic prediction and control of autonomous vehicles on highways. An interacting multiple model Kalman filter (IMM-KF)-related algorithm is applied to predict the motion behavior of the traffic participants by considering their interactions. A scenario generation component is used to produce plausible scenarios of the vehicles. A novel integrated decision-making and control system is proposed by applying a scenario-based model predictive control (MPC) approach. The designed controller considers safety, driving comfort, and traffic rules. The recursive feasibility of the controller is guaranteed under the inclusion of the "worst case" as an additional scenario to obtain safe inputs. Finally, the proposed scheme is evaluated under a high-fidelity IPG CarMaker and Simulink co-simulation environment. Simulation results indicate that the vehicle performs safe maneuvers under the designed control framework in different traffic situations.**

***Index Terms*— Decision-making, interacting multiple model Kalman filter (IMM-KF), IPG CarMaker, recursive feasibility, scenario-based model predictive control (MPC), traffic prediction and control.**

I. Introduction

A. Motivation

DESIGNING control systems for autonomous vehicles on highways has been extensively studied in recent decades. These systems primarily aim to safely control the ego vehicle (EV) by predicting the motion states of the surrounding target vehicles (TVs) [1]. The predicted states are usually uncertain, so generating safe, comfortable, energy-efficient, and real-time capable control strategies is challenging.

B. Literature Review

Physics-based [2], maneuver-based [3], and interaction-aware motion models [4], [5], [6] are used for the state prediction of vehicles. Since the interconnections between traffic participants are considered in interaction-aware models, they are a good choice for describing realistic scenarios. Specifically, the mutual influence of the vehicles is usually expressed from a finite set of trajectory clusters or dynamic Bayesian networks (DBNs) [7], [8]. Moreover, a novel interaction-aware traffic model is proposed by Lefkopoulos et al. [9], combining the physics of the vehicles, the intention of the drivers, and a no-collision assumption using an interacting multiple model Kalman filter (IMM-KF).

Model predictive control (MPC) has been widely used to control the EV by considering multiple constraints [10], [11], [12]. The reason for the prevalence of MPC is its ability to handle explicit constraints in an optimization problem with a moving horizon [13]. As a variant of stochastic MPC, scenario-based MPC (SCMPC) has been successfully implemented for various highway traffic conditions, as it is easily compatible with the traffic prediction component and can handle uncertainty based on only a small number of scenarios [14].

To model the interaction between vehicles over the MPC prediction horizon, the EV's motion is modeled as a stochastic process, and the mode transition is modeled as a Markov chain in [15] and [16]. The transition model is either learned or estimated using the previous EV and TVs measurements. A stochastic safety guarantee for the EV is introduced in [17] based on the TVs' motion behavior, where a set of possible TV trajectories is obtained by training the predictive model in a given scenario. A branch MPC is proposed in [18], where a scenario tree and a trajectory tree are applied to represent the possible motion behavior of the EV and TVs. The branch probability of two trees influences each other based on their interactions. In another approach, a trajectory prediction method is represented by learning the fused EV and TVs model considering their mutual influence inside MPC [19].

Safety is one of the most critical aspects of controlling the EV. This feature becomes more challenging in emergency scenarios, e.g., an unexpected deceleration of the leading vehicle (LV) or a sudden cut-in of a TV. These circumstances are identified as a safety-critical event (SCE) [20], where the EV immediately brakes against the crash, which may lead to a deceleration until a standstill [21]. Adaptive cruise control (ACC) is an example of a driver assistance system for resolving SCEs, where the EV reacts based on the information about the LV. However, a large time headway in this algorithm may lead to overconservative actions [22]. A safety controller is proposed based on ACC in [23], where the EV uses a predefined deceleration profile. Another representative solution to SCEs is the rigorous formalizing mathematical model of responsibility-sensitive safety (RSS) [24]. In this

Received 10 January 2024; revised 10 January 2024 and 24 April 2024; accepted 29 July 2024. Date of publication 25 September 2024; date of current version 26 June 2025. This work was supported by Deutsche Forschungsgemeinschaft (DFG), German Research Foundation, under Project 460891204. Recommended by Associate Editor Jana Tumova. *(Corresponding author: Xiaorong Zhang.)*

The authors are with the Institute for Electrical Engineering in Medicine, University of Luebeck, 23562 Luebeck, Germany (e-mail: x.zhang@student.uni-luebeck.de; sahar.zeinali@uni-luebeck.de; georg.schildbach@uni-luebeck.de).

Digital Object Identifier 10.1109/TCST.2024.3458817

model, a safety distance is defined by assuming a "worst case" scenario, and the EV responds to an SCE by decelerating at a predefined rate without full braking. This approach might be sensitive to the parameter design, and the subtle change of the parameter set might lead to a different decision strategy [25].

C. Contribution

Considering interaction between vehicles and generating traffic scenarios within MPC make the problem complicated and computationally costly. To solve this challenge, we apply a computation-efficient IMM-KF to produce possible interaction-aware scenarios [9]. Then, the scenarios obtained are considered in SCMPC to compute collision-free actions for the EV. Unlike the methods, which include the decision-making of lane change for the EV during the interaction process in [15], [16], [17], [18], and [19], two control modes, i.e., "lane keeping" and "lane change," are proposed in this article to decrease the complexity of the problem by excluding the decision-making process of the EV. To guarantee the safety of the control actions, inspired by the idea of the contingency MPC in [19], the "worst case" scenario is introduced into the SCMPC formulation, and the recursive feasibility of the SCMPC is proved, accordingly. Compared with our previous work in [26], in this article, the proposed approach is extensively validated for different scenarios in a realistic environment, IPG CarMaker, in which a high-fidelity model of the EV and interaction-aware motion models of TVs are used. The computed control inputs from SCMPC are converted to the appropriate actions, engine/brake torque, or steering angle by applying a proportional–derivative (PD) controller plus the feedforward compensation. The simulation results indicate that the EV performs safe and desirable maneuvers by applying the designed control architecture.

II. Control Architecture

The proposed control architecture is shown in Fig. 1 and works as follows. First, the motion states of the TVs and the EV are predicted based on the IMM-KF. Part of this information is sent to a scenario generation component to produce all possible maneuvers of the TVs. Then, the most likely scenarios are filtered based on a predefined probability threshold. Finally, an SCMPC-based control system consisting of two control modes is established, which corresponds to "following the current lane" or "changing the lane." In addition to the filtered scenarios, the "worst case" scenario is also included in the design of both controllers. A decision-making module chooses the desired inputs for the EV based on the cost function value of the two control modes. The computed control inputs are converted to the proper variables for the actuators of the IPG CarMaker, i.e., engine torque or brake torque and steering angle, and then applied to the EV.

III. Scenario Generation

A. Intention-Based Policy Mode

In contrast to many driver assistance systems, such as ACC, autonomous driving on highways requires the EV to consider

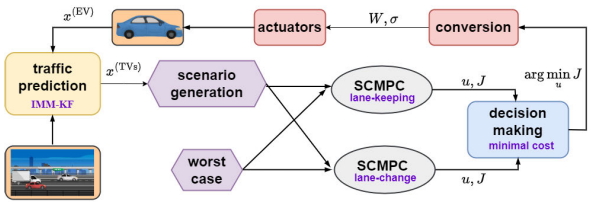

Fig. 1. Schematic of the proposed control structure.

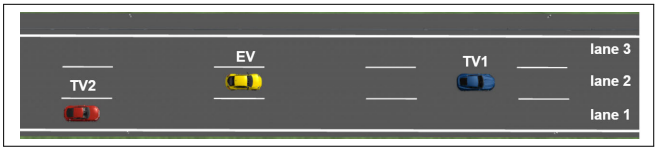

Fig. 2. Illustration of lanes and vehicles.

multiple TVs simultaneously. The TVs are numbered as TV1, TV2, and so on, where the LV is always referred to as TV1, the front vehicle of the EV, throughout this article. In the longitudinal direction, the velocity tracking (VT) and distance keeping (DK) policy modes are used. The vehicle tracks a reference velocity in VT while keeping a safe distance from its LV in DK [9]. In the lateral direction, three policy modes corresponding to "lane 1," "lane 2," and "lane 3" represent the target lanes of the vehicles, as shown in Fig. 2. Thus, the total number of modes M is 6.

The common state vector x_k in all modes at time k is

$$x_k \triangleq \Big[\underbrace{p_{\text{lon},k} \quad v_{\text{lon},k} \quad a_{\text{lon},k}}_{x_{\text{lon},k}} \quad \underbrace{p_{\text{lat},k} \quad v_{\text{lat},k} \quad a_{\text{lat},k}}_{x_{\text{lat},k}}\Big]^\top \tag{1}$$

where $p_{*,k}, v_{*,k}$, and $a_{*,k}$ are the position, velocity, and acceleration in the corresponding direction, respectively, $* \in \{\text{lon}, \text{lat}\}$. The unknown reference variable $r_{\text{ref},k}$, i.e., reference velocity $v_{\text{ref},k}$ or the reference time gap $t_{\text{gap},k}$, is also included in the longitudinal policy mode to be estimated. Therefore, the full state vector z_k in each policy mode at time k is

$$z_k \triangleq \Big[\underbrace{x_{\text{lon},k} \quad r_{\text{ref},k}}_{z_{\text{lon},k}} \quad \underbrace{x_{\text{lat},k}}_{z_{\text{lat},k}}\Big]^\top. \tag{2}$$

Note that we use $x_k^{(\circledast)}$ or $z_k^{(\circledast)}$ to clarify the common or full state of a specific vehicle, where $\circledast \in \{\text{EV}, \text{TV}, \text{LV}\}$. To make the policies closer to the driver's real intention, two linear quadratic regulator (LQR)-based feedback controllers are included in longitudinal and lateral policy modes. The associated control gains are defined as follows:

$$K_{\text{lon}}^{(\diamond)} = \begin{bmatrix} K_{\text{lon},1}^{(\diamond)} & K_{\text{lon},2}^{(\diamond)} & K_{\text{lon},3}^{(\diamond)} \end{bmatrix}^\top \tag{3a}$$

$$K_{\text{lat}} = \begin{bmatrix} K_{\text{lat},1} & K_{\text{lat},2} & K_{\text{lat},3} \end{bmatrix}^\top \tag{3b}$$

where $\diamond \in \{\text{VT}, \text{DK}\}$. Denoting the sampling time as T, the discrete form of each policy mode at time k is

$$\underbrace{\begin{bmatrix} z_{\text{lon},k+1} \\ z_{\text{lat},k+1} \end{bmatrix}}_{z_{k+1}} = \underbrace{\begin{bmatrix} F_{\text{lon},k}^{(\diamond)} & \mathbf{0}_{4\times 3} \\ \mathbf{0}_{3\times 4} & F_{\text{lat},k}^{(\lambda)} \end{bmatrix}}_{F_k} \underbrace{\begin{bmatrix} z_{\text{lon},k} \\ z_{\text{lat},k} \end{bmatrix}}_{z_k} + \underbrace{\begin{bmatrix} E_{\text{lon},k}^{(\diamond)} \\ E_{\text{lat},k}^{(\lambda)} \end{bmatrix}}_{E_k} + \omega_k \tag{4a}$$

$$y_k = \boldsymbol{I}_{7\times 7} z_k + v_k \tag{4b}$$

where $y_k \in \mathbb{R}^7$ and $\boldsymbol{I}_{7\times7}$ are the measurement vector and observation matrix. ω_k and ν_k are assumed to be normally distributed process noise and measurement noise, with the covariances Q and R. The longitudinal system matrices are

$$F_{\text{lon},k}^{(\text{VT})} = \begin{bmatrix} 1 & T & \frac{T^2}{2} & 0 \\ 0 & 1-\frac{K_{\text{lon},2}^{(\text{VT})}T^2}{2} & T-\frac{K_{\text{lon},3}^{(\text{VT})}T^2}{2} & \frac{K_{\text{lon},2}^{(\text{VT})}T^2}{2} \\ 0 & -K_{\text{lon},2}^{(\text{VT})}T & 1-K_{\text{lon},3}^{(\text{VT})}T & K_{\text{lon},2}^{(\text{VT})}T \\ 0 & 0 & 0 & 1 \end{bmatrix}$$

$$F_{\text{lon},k}^{(\text{DK})} = \begin{bmatrix} 1-\frac{K_{\text{lon},1}^{(\text{DK})}T^3}{6} & -\frac{K_{\text{lon},1}^{(\text{DK})}T^2}{2} & -K_{\text{lon},1}^{(\text{DK})}T & 0 \\ T-\frac{K_{\text{lon},2}^{(\text{DK})}T^3}{6} & 1-\frac{K_{\text{lon},2}^{(\text{DK})}T^2}{2} & -K_{\text{lon},2}^{(\text{DK})}T & 0 \\ \frac{T^2}{2}-\frac{K_{\text{lon},3}^{(\text{DK})}T^3}{6} & T-\frac{K_{\text{lon},3}^{(\text{DK})}T^2}{2} & 1-K_{\text{lon},3}^{(\text{DK})}T & 0 \\ -\frac{K_{\text{lon},1}^{(\text{DK})}v_{\text{lead},k}T^3}{6} & -\frac{K_{\text{lon},1}^{(\text{DK})}v_{\text{lead},k}T^2}{2} & -K_{\text{lon},2}^{(\text{DK})}v_{\text{lead},k}T & 1 \end{bmatrix}^\top$$

and the LQR-related input matrices are

$$E_{\text{lon},k}^{(\text{VT})} = \boldsymbol{0}_{4\times1}$$

$$E_{\text{lon},k}^{(\text{DK})} = \begin{bmatrix} \frac{K_{\text{lon},1}^{(\text{DK})}T^3}{6}-1 & \frac{K_{\text{lon},2}^{(\text{DK})}T^3}{6}-T & \frac{K_{\text{lon},3}^{(\text{DK})}T^3}{6}-\frac{T^2}{2} & 0 \\ \frac{K_{\text{lon},1}^{(\text{DK})}T^2}{2} & \frac{K_{\text{lon},2}^{(\text{DK})}T^2}{2}-1 & \frac{K_{\text{lon},3}^{(\text{DK})}T^2}{2}-T & 0 \\ K_{\text{lon},1}^{(\text{DK})}T & K_{\text{lon},2}^{(\text{DK})}T & K_{\text{lon},3}^{(\text{DK})}T-1 & 0 \\ 0 & 0 & 0 & 0 \end{bmatrix} \times \begin{bmatrix} p_{\text{lon},k}^{(\text{LV})} \\ v_{\text{lon},k}^{(\text{LV})} \\ a_{\text{lon},k}^{(\text{LV})} \\ 0 \end{bmatrix}.$$

Considering the position $p^{(\lambda)}$ of the center line of the target lane λ, $\lambda \in \{1, 2, 3\}$, the lateral system and input matrices are

$$F_{\text{lat},k}^{(\lambda)} = \begin{bmatrix} -\frac{K_{\text{lat},1}T^3}{6} & -\frac{K_{\text{lat},2}T^3}{6} & -\frac{K_{\text{lat},3}T^3}{6} \\ -\frac{K_{\text{lat},1}T^2}{2} & -\frac{K_{\text{lat},2}T^2}{2} & -\frac{K_{\text{lat},3}T^2}{2} \\ -K_{\text{lat},1}T & -K_{\text{lat},2}T & -K_{\text{lat},3}T-1 \end{bmatrix} \tag{5a}$$

$$E_{\text{lat},k}^{(\lambda)} = \begin{bmatrix} \frac{K_{\text{lat},1}T^3}{6}p^{(\lambda)} \\ \frac{K_{\text{lat},1}T^2}{2}p^{(\lambda)} \\ K_{\text{lat},1}Tp^{(\lambda)} \end{bmatrix}. \tag{5b}$$

B. Interaction-Aware Estimation and Prediction

Each vehicle's state estimation and prediction are calculated in descending priority order based on vehicles' interactions. The priority criteria are as follows: 1) if two vehicles are in the same lane, the preceding one has higher priority and 2) if two vehicles are in different lanes, the one with the higher longitudinal progress over a specific horizon has higher priority [9].

For the sake of clarity, a policy mode corresponds to one model of the IMM-KF in this work. In the IMM-KF, we consider the Markov jump linear system (4), where the transition probability from mode i to mode j is denoted as $\pi^{(i|j)} \in [0, 1]$, $i, j \in \{1, 2, \ldots, 6\}$. Since the reference parameters of the VT and DK modes are different, we mix individual common estimates and initialize each mode in the first step as follows:

$$c^{(i)} = \sum_{j=1}^{M} \pi^{(j|i)}\mu_{k-1}^{(j)} \tag{6a}$$

$$\mu_{k-1}^{(j|i)-} = \frac{\pi^{(j|i)}\mu_{k-1}^{(j)}}{c^{(i)}} \tag{6b}$$

$$\bar{x}_{k-1}^{(i)-} = \sum_{j=1}^{M} \mu_{k-1}^{(j|i)-}\hat{x}_{k-1}^{(j)-} \tag{6c}$$

$$\bar{P}_{k-1}^{(i)-} = \sum_{j=1}^{M} \mu_{k-1}^{(j|i)-}\Big[P_{k-1}^{(j)-} + \Big(\bar{x}_{k-1}^{(i)-} - \hat{x}_{k-1}^{(j)-}\Big) \times \Big(\bar{x}_{k-1}^{(i)-} - \hat{x}_{k-1}^{(j)-}\Big)^\top\Big] \tag{6d}$$

where $\mu_{k-1}^{(j|i)-}$ is the mixing conditional mode probability, and $\hat{x}_{k-1}^{(j)-}$ and $P_{k-1}^{(j)-}$ are the common state estimation and covariance, which are part of the full state estimation $\hat{z}_{k-1}^{(j)-}$ and covariance $\mathbb{P}_{k-1}^{(j)-}$. The fused common state estimation and covariance are $\bar{x}_{k-1}^{(i)-}$ and $\bar{P}_{k-1}^{(i)-}$. $\bar{z}_{k-1}^{(i)-}$ and $\bar{\mathbb{P}}_{k-1}^{(i)-}$ are fused full state estimation and covariance. Then, each mode is predicted and updated as follows:

$$\hat{z}_{k-1}^{(i)+} = F_{k-1}^{(i)}\bar{z}_{k-1}^{(i)-} + E_{k-1}^{(i)} \tag{7a}$$

$$\mathbb{P}_{k-1}^{(i)+} = F_{k-1}^{(i)}\bar{\mathbb{P}}_{k-1}^{(i)-}F_{k-1}^{(i)\top} + Q_{k-1}^{(i)} \tag{7b}$$

$$\tilde{y}_k^{(i)} = y_k^{(i)} - \boldsymbol{I}_{7\times7}\hat{z}_{k-1}^{(i)+} \tag{7c}$$

$$r_k^{(i)} = \boldsymbol{I}_{7\times7}\mathbb{P}_{k-1}^{(i)+}\boldsymbol{I}_{7\times7}^\top + R_k^{(i)} \tag{7d}$$

$$L_k^{(i)} = \mathbb{P}_{k-1}^{(i)+}\boldsymbol{I}_{7\times7}^\top r_k^{(i)-1} \tag{7e}$$

$$\hat{z}_k^{(i)-} = \hat{z}_{k-1}^{(i)+} + L_k^{(i)}\tilde{y}_k^{(i)} \tag{7f}$$

$$\mathbb{P}_k^{(i)-} = \big(\boldsymbol{I}_{7\times7} - L_k^{(i)}\boldsymbol{I}_{7\times7}\big)\mathbb{P}_{k-1}^{(i)+} \tag{7g}$$

with the prior state estimate $\hat{z}_{k-1}^{(i)+}$ and covariance $\mathbb{P}_{k-1}^{(i)+}$, the innovation residual $\tilde{y}_k^{(i)}$ and its covariance $r_k^{(i)}$, Kalman gain $L_k^{(i)}$, and posterior predicted state estimate $\hat{z}_k^{(i)-}$ and covariance $\mathbb{P}_k^{(i)-}$.

To obtain the no-collision prediction, a mixed integer quadratic programming (MIQP) problem is formulated to obtain the modified state estimation $\hat{z}_k^{(\text{proj})-}$ as follows:

$$\min_{\hat{z}_k^{(\text{proj})-}} \left\|\hat{z}_k^{(\text{proj})-} - \hat{z}_k^{-}\right\|_{\bar{W}} \tag{8a}$$

$$\text{s.t. } \hat{z}_{t|k} = \phi(t, 1)\hat{z}_k^{-} + \sum_{\delta=k+1}^{t} \phi(t, \delta)E_{\delta-1} \tag{8b}$$

$$\phi(t,\delta)=\begin{cases}\left(\Pi_{\eta=\delta}^{t-1}F_\eta^\top\right)^\top, & \text{if } t>\delta\\ \boldsymbol{I}_{7\times7}, & \text{if } t=\delta\end{cases} \tag{8c}$$

$$\bigwedge_{t\in\{k,k+1,\ldots,k+N\}}\left|\hat{p}_{\text{lon},t|k}-p_{\text{lon},t|k}^{(\circ)}\right|\geq\frac{h+h^{(\circ)}}{2}$$

$$\text{if }\left|\hat{p}_{\text{lat},t|k}-p_{\text{lat},t|k}^{(\circ)}\right|\leq\frac{w+w^{(\circ)}}{2} \tag{8d}$$

where $\bar{W}\succ 0$ is chosen based on the goal of primarily modifying the reference state estimate $r_{\text{ref},k}$. h and w are the vehicle's length and width, respectively. The safety constraints over the prediction horizon N between the studied vehicle and other vehicles $\circ\in\circledast$ in the same lane are considered. Note that the state estimation of each policy mode is still $\hat{z}_k^-$, and the state estimation error between $\hat{z}_k^-$ and $\hat{z}_k^{(\text{proj})-}$, and its covariance are used to augment the innovation residual $\bar{y}_k^{(i)}$ and its covariance $r_k{}^{(i)}$ as $\breve{y}_k^{(i)}$ and $\tilde{r}_k{}^{(i)}$. Then, the policy mode probability is updated based on the augmented matrices

$$\tilde{L}_k^{(i)}=\frac{\exp\left(-\frac{1}{2}\breve{y}_k^{(i)\top}\tilde{r}_k{}^{(i)-1}\breve{y}_k^{(i)}\right)}{\left|2\pi\tilde{r}_k^{(i)}\right|^{1/2}} \tag{9a}$$

$$\tilde{\mu}_k^{(i)}=\frac{c^{(i)}\tilde{L}_k^{(i)}}{\sum_{j=1}^{M}c^{(j)}\tilde{L}_k^{(j)}}. \tag{9b}$$

The final step is to mix state estimation and its covariance according to the updated probability of the individual mode

$$\hat{x}_k^-=\sum_{i=1}^{M}\tilde{\mu}_k^{(i)}\hat{x}_k^{(i)-} \tag{10a}$$

$$P_k^-=\sum_{i=1}^{M}\tilde{\mu}_k^{(i)}\left[P_k^{(i)-}+\left(\hat{x}_k^--\hat{x}_k^{(i)-}\right)\left(\hat{x}_k^--\hat{x}_k^{(i)-}\right)^\top\right]. \tag{10b}$$

For no-collision intention, the updated state estimation $\hat{x}_k^-$ along with $r_{\text{ref},k}^{(i)}$ is modified from an MIQP problem, such as (8). Then, the updated state is used to predict each policy mode's state in terms of (8b) and (8c).

C. Scenario Generation of TVs

A scenario is defined as a tuple of motion maneuvers for all TVs. Assuming that the number of investigated TVs is V, then a total of M^V possible scenarios can be generated. $\mu_i^{(n)}$ is the probability of TV n with the policy mode i, $i\in\{1,2,\ldots,6\}$. Assuming statistical independence of each vehicle's no-collision prediction over the prediction horizon, then the probability of the scenario s is calculated by

$$\Pr(s)=\prod_{n=1}^{V}\mu_i^{(n)},\quad s=1,\ldots,M^V \tag{11}$$

where $\sum_{s=1}^{M^V}\Pr(s)=1$. In order to focus only on the most relevant scenarios, scenarios with a probability less than a predefined threshold $\underline{P}$ are not considered. The probability of the remaining scenarios is normalized by

$$\overline{\Pr}(s)=\frac{\Pr(s)}{1-\sum_{\zeta=1}^{\theta}\Pr(\zeta)},\quad s=1,\ldots,M^V-\theta \tag{12}$$

where θ is the total number of scenarios with probability less than $\underline{P}$.

IV. Scenario-Based MPC

Based on the predicted scenarios of the TVs, a feasible trajectory for the EV is calculated by solving a constrained finite-time optimal control problem (CFTOCP) in a moving horizon fashion. The objective of the optimization problem is to follow the planned reference trajectory with minimum effort while considering safety constraints, traffic rules, and driving comfort. The first computed control input of the CFTOCP is fed to the system at each time step.

A. Vehicle Model

A triple integrator is used as the EV's motion model in both longitudinal and lateral directions

$$\underbrace{\begin{bmatrix}p_{*,k+1}^{(\text{EV})}\\ v_{*,k+1}^{(\text{EV})}\\ a_{*,k+1}^{(\text{EV})}\end{bmatrix}}_{x_{*,k+1}^{(\text{EV})}}=\underbrace{\begin{bmatrix}1 & T_\text{p} & \frac{1}{2}T_\text{p}{}^2\\ 0 & 1 & T_\text{p}\\ 0 & 0 & 1\end{bmatrix}}_{A}\underbrace{\begin{bmatrix}p_{*,k}^{(\text{EV})}\\ v_{*,k}^{(\text{EV})}\\ a_{*,k}^{(\text{EV})}\end{bmatrix}}_{x_{*,k}^{(\text{EV})}}+\underbrace{\begin{bmatrix}\frac{1}{6}T_\text{p}{}^3\\ \frac{1}{2}T_\text{p}{}^2\\ T_\text{p}\end{bmatrix}}_{B}\underbrace{j_{*,k}^{(\text{EV})}}_{u_{*,k}^{(\text{EV})}} \tag{13}$$

with the prediction time step T_p. Equation (13) can be rewritten as follows:

$$x_{k+1}^{(\text{EV})}=\underbrace{\begin{bmatrix}A & 0_{3\times3}\\ 0_{3\times3} & A\end{bmatrix}}_{\bar{A}}x_k^{(\text{EV})}+\underbrace{\begin{bmatrix}B\\ B\end{bmatrix}}_{\bar{B}}u_k^{(\text{EV})}. \tag{14}$$

B. Scenario-Based Model Predictive Controller

The proposed SCMPC scheme has two control modes as follows: 1) the EV stays in the current lane and keeps its velocity and 2) the EV switches to the target lane and keeps its velocity. For each control mode, a CFTOCP is solved for a corresponding reference trajectory. The decision-making module then selects the control mode with the lower cost.

In addition to generated scenarios, a so-called "worst case" scenario is introduced to ensure the recursive feasibility of CFTOCP. In this scenario, the LV is assumed to decelerate with its minimum acceleration over the prediction horizon. We introduce two sequences of control inputs $u_0^{(\text{EV})},\ldots,u_{N-1}^{(\text{EV})}$ and $\breve{u}_0^{(\text{EV})},\ldots,\breve{u}_{N-1}^{(\text{EV})}$. The first input sequence is calculated to avoid collision between the EV and the LV/TVs under the generated scenarios and to evaluate the cost function with associated states $x_k^{(\text{EV})}$. The second sequence is obtained by considering the safety constraints under the "worst case" scenario, with associated states $\breve{x}_k^{(\text{EV})}$, and the terminal set of the states $\breve{\mathbb{X}}_f^{(\text{EV})}$, detailed in Section IV-D. The first computed inputs $u_0^{(\text{EV})}$ and $\breve{u}_0^{(\text{EV})}$ must be equal to guarantee the recursive feasibility. The CFTOCP is formulated as follows:

$$J=\min_{u_k^{(\text{EV})},x_{k+1}^{(\text{EV})}}\sum_{k=0}^{N-1}\left\|x_{k+1}^{(\text{EV})}-x_{\text{ref},k+1}^{(\text{EV})}\right\|_{\bar{Q}}+\left\|u_k^{(\text{EV})}\right\|_{\bar{R}} \tag{15a}$$

$$\text{s.t. } x_{k+1}^{(\text{EV})}=f(x_k^{(\text{EV})},u_k^{(\text{EV})}),\quad k=0,1,\ldots,N-1 \tag{15b}$$

$$\breve{x}_{k+1}^{(\text{EV})}=f(\breve{x}_k^{(\text{EV})},\breve{u}_k^{(\text{EV})}),\quad k=0,1,\ldots,N-1 \tag{15c}$$

$$x_k^{(\mathrm{EV})} \in \mathbb{X}^{(\mathrm{EV})}, \quad \breve{x}_k^{(\mathrm{EV})} \in \breve{\mathbb{X}}^{(\mathrm{EV})} \quad k = 0, 1, \ldots, N-1 \tag{15d}$$

$$u_k^{(\mathrm{EV})} \in \mathbb{U}^{(\mathrm{EV})}, \quad \breve{u}_k^{(\mathrm{EV})} \in \breve{\mathbb{U}}^{(\mathrm{EV})} \quad k = 0, 1, \ldots, N-1 \tag{15e}$$

$$u_0^{(\mathrm{EV})} = \breve{u}_0^{(\mathrm{EV})} \tag{15f}$$

$$\breve{x}_N^{(\mathrm{EV})} \in \breve{\mathbb{X}}_f^{(\mathrm{EV})} \tag{15g}$$

$$x_0^{(\mathrm{EV})} = \breve{x}_0^{(\mathrm{EV})} = x^{(\mathrm{EV})}(0). \tag{15h}$$

Here, $x_{\mathrm{ref},k+1}^{(\mathrm{EV})}$ is the reference state based on the relevant control mode. In the lane-changing mode, we consider the EV to only change one lane according to the real traffic situation. Hence, the number of related reference trajectories depends on the current lane of the EV. $\bar{Q} \in \mathbb{R}^{6\times 6}$ and $\bar{R} \in \mathbb{R}^{2\times 2}$ are tunable positive definite weighting matrices. The feasible state sets $\mathbb{X}^{(\mathrm{EV})}$ and $\breve{\mathbb{X}}^{(\mathrm{EV})}$ and input set $\mathbb{U}^{(\mathrm{EV})}$ and $\breve{\mathbb{U}}^{(\mathrm{EV})}$ are limited by appropriate constraints, as detailed below.

Remark 1: If there is no LV in reality, it is assumed that there is an LV far away from the EV.

Remark 2: Once the lane-changing mode is activated, it stays active until the lane-changing maneuvers are completed. For SCMPC in lane-changing mode, except for considering the "worst case" scenario of the LV in the target lane, the "worst case" scenario of the LV in the previous lane is also considered during the EV's lane change.

C. Constraints

1) State and Input Constraints: The EV's motion state and action are limited by traffic rules and driving comfort. The lateral position is constrained by the lane bounds $[l_{\mathrm{ub}}, l_{\mathrm{lb}}]$

$$0 < v_{\mathrm{lon},k}^{(\mathrm{EV})}, \quad l_{\mathrm{lb}} \le p_{\mathrm{lat},k}^{(\mathrm{EV})} \le l_{\mathrm{ub}} \tag{16a}$$

$$\underline{a}_{\mathrm{lon}} \le a_{\mathrm{lon},k}^{(\mathrm{EV})} \le \overline{a}_{\mathrm{lon}}, \quad \underline{a}_{\mathrm{lat}} \le a_{\mathrm{lat},k}^{(\mathrm{EV})} \le \overline{a}_{\mathrm{lat}} \tag{16b}$$

$$\underline{j}_{\mathrm{lon}} \le j_{\mathrm{lon},k}^{(\mathrm{EV})} \le \overline{j}_{\mathrm{lon}}, \quad \underline{j}_{\mathrm{lat}} \le j_{\mathrm{lat},k}^{(\mathrm{EV})} \le \overline{j}_{\mathrm{lat}} \tag{16c}$$

where $\underline{\bullet}$ and $\overline{\bullet}$ denote the minimum and maximum values of the associated variables.

2) Safety Constraints: A safe distance between the EV and the LV in the same lane is required

$$d_k \ge \underline{d} \tag{17}$$

and the safety distance $\underline{d}$ is computed by

$$\underline{d} = \tau v_{\mathrm{lon},k}^{(\mathrm{EV})} + \triangle d \tag{18}$$

with the design parameters τ and $\triangle d$ [27]. If the reference point of all vehicles is in their respective center, for example, choose $\triangle d \ge ((l^{(\mathrm{EV})} + l^{(\mathrm{LV})})/2)$, where $l^{(\mathrm{EV})}$ and $l^{(\mathrm{LV})}$ are the length of EV and LV. During the lane-changing period, in addition to keeping a safe distance from the LVs in both the current and target lane, the EV also maintains a safe distance with the TV behind it in the target lane. The required safety distance also satisfies (18). The safety constraint under the generated scenario is based on (18), while the safety distance for considering the "worst case" scenario collapses to $\triangle d$.

D. Recursive Feasibility of the SCMPC

Definition 1 (Recursive Feasibility): The SCMPC is recursively feasible if (17) always holds. Namely, in lane-keeping mode, a collision between the EV and the LV is always avoidable. In lane-changing mode, no accident occurs between the EV and the other vehicles during the lane-changing process, and then, the EV remains safe in the target lane.

If the safety constraints are met in the "worst case" scenario, it means that the EV can manage any traffic situation under the SCMPC. This capability is denoted by a parameter called the minimal stopping horizon $\underline{N}$, defined as follows.

Definition 2 (Minimal Stopping Horizon): Given the initial velocity $v_{\mathrm{lon},0}^{(\mathrm{EV})}$ and the minimal acceleration $\underline{a}_{\mathrm{lon}}^{(\mathrm{EV})}$ of the EV, the minimal stopping horizon $\underline{N} \in \mathbb{N}$ satisfies

$$\underline{N} = \left\lceil \frac{v_{\mathrm{lon},0}^{(\mathrm{EV})}}{\left|\underline{a}_{\mathrm{lon}}^{(\mathrm{EV})}\right| T_{\mathrm{p}}} \right\rceil \tag{19}$$

where $\lceil \bullet \rceil$ is defined as the smallest integer that is not smaller than a real number $\bullet$.

If we choose the prediction horizon $N \ge \underline{N}$, the terminal set $\breve{\mathbb{X}}_{\mathrm{f}}$ at the time t is

$$\breve{\mathbb{X}}_{\mathrm{f}}^{(\mathrm{EV})} \triangleq \left\{ \breve{x}_{N|t}^{(\mathrm{EV})} | \breve{x}_{N|t}^{(\mathrm{EV})} = \begin{bmatrix} p_{\mathrm{lon},\underline{N}|t}^{(\mathrm{EV})} & 0 & 0 & p^{(\lambda)} & 0 & 0 \end{bmatrix}^{\top} \right\} \tag{20}$$

where the stopping longitudinal position $p_{\mathrm{lon},\underline{N}|0}^{(\mathrm{EV})}$ of the EV is determined by its initial position $p_{\mathrm{lon},0}^{(\mathrm{EV})}$, initial velocity $v_{\mathrm{lon},0}^{(\mathrm{EV})}$, and minimal acceleration $\underline{a}_{\mathrm{lon}}^{(\mathrm{EV})}$. The terminal lateral position of the EV is the position of the center line of the target lane $p^{(\lambda)}$ under the specific control mode. Based on the general traffic situation and rules, we make the following assumptions.

Assumption 1: All vehicles only drive forward, and the EV is only responsible for front collisions.

Assumption 2: $u_k^{(\mathrm{EV})} = [0\ 0]^{\top}$ is one element of the feasible set $\breve{\mathbb{U}}$.

The recursive feasibility of the SCMPC can then be proved.

Theorem 1: If SCMPC is initially feasible, and the prediction horizon $N \ge \underline{N}$, then the controller is recursively feasible based on Assumptions 1 and 2.

Proof: Let two initial control inputs of the generated normal scenarios and the "worst case" scenario be $\{u_{0|0}^{(\mathrm{EV})}, u_{1|0}^{(\mathrm{EV})}, \ldots, u_{\underline{N}|0}^{(\mathrm{EV})}, \ldots, u_{N|0}^{(\mathrm{EV})}\}$ and $\{\breve{u}_{0|0}^{(\mathrm{EV})}, \breve{u}_{1|0}^{(\mathrm{EV})}, \ldots, \breve{u}_{\underline{N}|0}^{(\mathrm{EV})}, \ldots, \breve{u}_{N|0}^{(\mathrm{EV})}\}$. Choose the second control sequence as initially feasible solution $\{\breve{u}_{0|0}^{(\mathrm{EV})\star}, \breve{u}_{1|0}^{(\mathrm{EV})\star}, \ldots, \breve{u}_{\underline{N}|0}^{(\mathrm{EV})\star}, \ldots, \breve{u}_{N|0}^{(\mathrm{EV})\star}\}$, and its related state sequence is $\{\breve{x}_{0|0}^{(\mathrm{EV})\star}, \breve{x}_{1|0}^{(\mathrm{EV})\star}, \ldots, \breve{x}_{\underline{N}|0}^{(\mathrm{EV})\star}, \ldots, \breve{x}_{N|0}^{(\mathrm{EV})\star}\}$. The terminal state $\breve{x}_{N|0}^{(\mathrm{EV})\star}$ is determined according to (20). We apply $\breve{u}_{0|0}^{(\mathrm{EV})\star}$ to system (14) and obtain

$$x_1^{(\mathrm{EV})} = \bar{A} x_0^{(\mathrm{EV})} + \bar{B} \breve{u}_{0|0}^{(\mathrm{EV})\star} = \breve{x}_{1|0}^{(\mathrm{EV})\star}. \tag{21}$$

Then, the following is a feasible solution for the MPC problem initialized at $x_1^{(\mathrm{EV})}$:

$$\begin{aligned} &\left\{ {u^{(\mathrm{EV})}}_{1|1}, {u^{(\mathrm{EV})}}_{2|1}, \ldots, {u^{(\mathrm{EV})}}_{\underline{N}|1}, \ldots, {u^{(\mathrm{EV})}}_{N-1|1}, u_{N|1}^{(\mathrm{EV})} \right\} \\ &= \left\{ \breve{u}_{1|0}^{(\mathrm{EV})\star}, \breve{u}_{2|0}^{(\mathrm{EV})\star}, \ldots, \breve{u}_{\underline{N}|0}^{(\mathrm{EV})\star}, \ldots, \breve{u}_{N-1|0}^{(\mathrm{EV})\star}, \begin{bmatrix} 0 & 0 \end{bmatrix}^{\top} \right\} \end{aligned} \tag{22}$$

where $[0\ 0]^\top \in \breve{\mathbb{U}}^{(\mathrm{EV})}$. The related state sequence is

$$\begin{aligned}&\left\{x_{2|1}^{(\mathrm{EV})}, x_{3|1}^{(\mathrm{EV})}, \ldots, x_{\underline{N}+1|1}^{(\mathrm{EV})}, \ldots, x_{N|1}^{(\mathrm{EV})}, x_{N+1|1}^{(\mathrm{EV})}\right\}\\ &=\left\{\breve{x}_{2|0}^{(\mathrm{EV})\star}, \breve{x}_{3|0}^{(\mathrm{EV})\star}, \ldots, \breve{x}_{\underline{N}|0}^{(\mathrm{EV})\star}, \ldots, \breve{x}_{N|0}^{(\mathrm{EV})\star}, \bar{A}\breve{x}_{N|0}^{(\mathrm{EV})\star}\right.\\ &\qquad\left.+\bar{B}\cdot\begin{bmatrix}0 & 0\end{bmatrix}^\top\right\}\end{aligned} \tag{23}$$

where $\bar{A}\breve{x}_{N|0}^{(\mathrm{EV})\star} + \bar{B}\cdot[0\ 0]^\top = \breve{x}_{N|0}^{(\mathrm{EV})\star}$. Both sequences are feasible for the MPC problem, because they satisfy the dynamics and the constraints. □

Remark 3: The conservativeness of the applied control action depends on the motion behavior of the LV. If the actual motion behavior of the LV is close to the "worst case" scenario, the control action is not conservative. Moreover, since only one-step control action of $u_0^{(\mathrm{EV})}$ and $\breve{u}_0^{(\mathrm{EV})}$ is identical to each other, this makes the control action less conservative.

V. Control Inputs Conversion

In IPG CarMaker, a real vehicle is represented by a simulated vehicle as the EV. To apply the control inputs longitudinal jerk $u_{\mathrm{lon},k}^{(\mathrm{EV})}$ and lateral jerk $u_{\mathrm{lat},k}^{(\mathrm{EV})}$ to the EV, they need to be converted into actions appropriate for the actuator, i.e., the engine torque or brake torque and steering angle. In particular, the considered longitudinal conversion model is

$$a_{\mathrm{lon},k}^{(\mathrm{EV})} = \frac{i_{g,k}\xi}{m r_\omega} W_k. \tag{24}$$

Here, $i_{g,k}$ represents the time-varying gear ratio, ξ is the transmission efficiency, m is the vehicle's overall mass, and r_w denotes the wheel radius. When $a_{\mathrm{lon},k}^{(\mathrm{EV})} > -0.2\ \mathrm{m/s^2}$, W_k represents the engine torque. Otherwise, it represents the brake torque. In IPG CarMaker, the range of the values for gas and brake is in $[0, 1]$, so the calculated engine or brake torque is divided by the related maximal value before being applied.

Based on the calculated $u_{\mathrm{lat},k}^{(\mathrm{EV})}$, the desired lateral states $\bar{p}_{\mathrm{lat},k}^{(\mathrm{EV})}$, $\bar{v}_{\mathrm{lat},k}^{(\mathrm{EV})}$, and $\bar{a}_{\mathrm{lat},k}^{(\mathrm{EV})}$ are obtained by a triple integrator model with the sampling time T_p. The steering angle σ_k is computed from a PD controller plus the feedforward compensation by considering the lateral position error as follows:

$$\sigma_k = K_\mathrm{P} e_{\mathrm{lat},k}^{(\mathrm{EV})} + K_\mathrm{D}\frac{de_{\mathrm{lat},k}^{(\mathrm{EV})}}{dt} + \bar{a}_{\mathrm{lat},k}^{(\mathrm{EV})} \tag{25a}$$

$$e_{\mathrm{lat},k}^{(\mathrm{EV})} = p_{\mathrm{lat},k}^{(\mathrm{EV})} - \bar{p}_{\mathrm{lat},k}^{(\mathrm{EV})} \tag{25b}$$

where $e_{\mathrm{lat},k}^{(\mathrm{EV})}$ is the lateral position error, which shows the deviation of the EV's real position from the desired one. K_P and K_D are the PD control gains for tuning.

VI. Simulation and Discussion

The presented approach is evaluated in three different traffic cases by controlling the EV under a high-fidelity environment, IPG CarMaker. The motion maneuvers of the TVs are executed based on Human Driver Models. We use DemoCar as the EV, IPG CompanyCar 2018 Blue, and Audi TT 2015 as the TVs.

A. Simulation Setup

To demonstrate the interaction awareness of traffic participants, we consider three different traffic scenarios, where the initial motion states of vehicles are set differently. Then, the TVs and the EV react differently to others. Specifically, when a slower vehicle is in front of a TV/EV, the latter might overtake or brake, depending on their relative distance, velocity, and surrounding vehicles. Therefore, these three cases, as comparisons with each other, are chosen to show the interaction results of vehicles from different perspectives. Table I shows the parameters used in the case studies. The total simulation time is denoted as t_s. The variable l_b represents the position of lane boundaries. Note that in the current simulation setup, if the EV is in lane 2, we only consider EV changes to lane 1, not to lane 1 or lane 3 in the lane-changing mode of the SCMPC. When the SCMPC is infeasible in a certain control mode, we set the corresponding cost function value to 150. Once the EV starts to change lanes, it will complete the lane change without being able to change the decision. We assume it enters the new lane within 4 s. The cost of the lane-keeping mode during this time is also set to 150.

TABLE I
Design Parameters Used in the Simulation Study

Parameter	t_s[s]	T[s]	T_p[s]
Value	30.00	0.40	0.40
Parameter	N	$\underline{a}_{\mathrm{lon}}^{(\mathrm{EV})}[\mathrm{m/s^2}]$	$\overline{a}_{\mathrm{lon}}^{(\mathrm{EV})}[\mathrm{m/s^2}]$
Value	15	-4.00	1.50
Parameter	$\underline{a}_{\mathrm{lat}}^{(\mathrm{EV})}[\mathrm{m/s^2}]$	$\overline{a}_{\mathrm{lat}}^{(\mathrm{EV})}[\mathrm{m/s^2}]$	$\underline{j}_{\mathrm{lon}}^{(\mathrm{EV})}[\mathrm{m/s^3}]$
Value	-2.00	2.00	-5.50
Parameter	$\overline{j}_{\mathrm{lon}}^{(\mathrm{EV})}[\mathrm{m/s^3}]$	$\underline{j}_{\mathrm{lat}}^{(\mathrm{EV})}[\mathrm{m/s^3}]$	$\overline{j}_{\mathrm{lat}}^{(\mathrm{EV})}[\mathrm{m/s^3}]$
Value	5.50	-4.00	4.00
Parameter	τ[s]	l_b[m]	$\underline{a}_{\mathrm{lon}}^{(\mathrm{LV})}[\mathrm{m/s^2}]$
Value	0.40	$\{-14, -10.25, -6.5, -2.75\}$	-4.00
Parameter	K_{lat}	$p_c^{(1),(2),(3)}$[m]	m[kg]
Value	$[1.15, 3.39, 3.58]^\top$	$\{-12.13, -8.38, -4.63\}$	1463.00
Parameter	$\{l_f, l_r\}$[m]	$h^{(\circledS)}$[m]	ξ
Value	$\{0.99, 1.54\}$	$\{4.47, 4.12, 4.28\}$	1.00
Parameter	r_ω[m]	$w^{(\circledS)}$[m]	P
Value	0.33	$\{1.97, 1.80, 1.80\}$	0.075
Parameter	$\bar{Q}$	$\bar{R}$	$\{K_\mathrm{P}, K_\mathrm{D}\}$
Value	$0.01 * \mathrm{diag}([10, 1, 1, 10, 1, 1])$	$\mathrm{diag}([0.1, 0.01])$	$\{0.5, 1.5\}$

Fig. 3. Initial traffic scene for Case 1.

B. Case 1 (EV Changes Lanes and Brakes)

Fig. 3 gives the initial traffic scene of Case 1. Specifically, the position, velocity, and acceleration of TV1, TV2, and EV are $x^{(\mathrm{TV1})} = [375, 20, 0, -8.38, 0, 0]^\top$, $x^{(\mathrm{TV2})} = [288, 20, 0, -12.13, 0, 0]^\top$, and $x^{(\mathrm{EV})} = [350, 18.9, 0, -8.38, 0, 0]^\top$, respectively. Given the initial traffic situation, TV1 keeps its speed in the first 5 s and then decelerates with $-4\ \mathrm{m/s^2}$ until 7 s and eventually returns to 20 m/s in the following time. The priority of the three vehicles is [TV1, EV, TV2] in descending order. Therefore, the EV reacts to TV1, and TV2 reacts to TV1 and the EV.

Figs. 4–7 show the simulated information of Case 1. From Fig. 7, we can see that the EV stays in lane 2 until 5.6 s due to a lower cost of lane-keeping mode. After that, as the lane-changing mode is less costly given that TV1 decelerates continuously, the EV changes to lane 1 at 8 s (as seen from Fig. 4). During the lane change, the EV decreases longitudinal velocity to around 17.5 m/s to avoid colliding with TV1. Then, the EV drives with this constant velocity for the rest of the

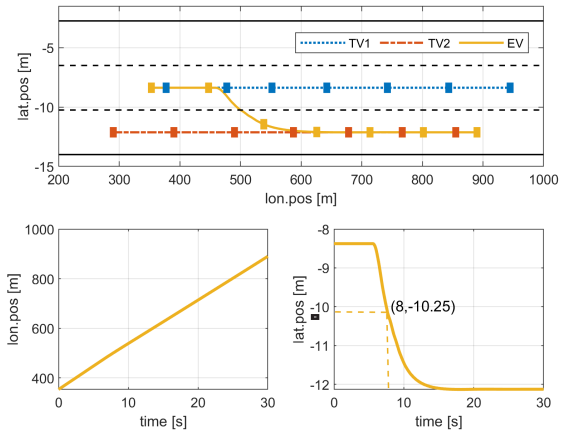

Fig. 4. Motion trajectories of all vehicles and the longitudinal and lateral positions of the EV for Case 1.

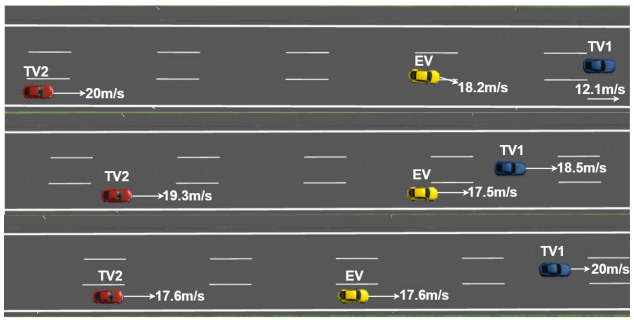

Fig. 5. Traffic scenes for Case 1 at 7.2, 13, and 24 s.

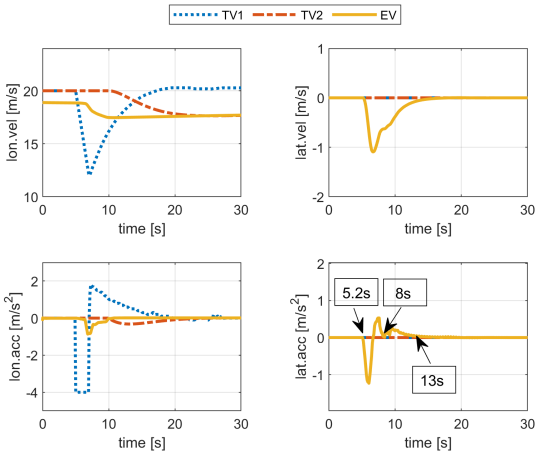

Fig. 6. Longitudinal and lateral velocities of all vehicles for Case 1.

time. As for TV2, as a vehicle behind the EV in the new lane, it decreases its velocity to the same velocity as the EV to maintain a safe distance from the EV.

Furthermore, the policy mode probabilities of TVs, as the basis of scenario generation, are provided and analyzed. Since the EV's policy mode probabilities influence the policy mode probability result of TV, whose priority is lower than the EV, its policy mode probabilities are also studied. The first three subplots of Fig. 8 show each vehicle's policy mode probabilities throughout the simulation time. The fourth subplot is the enlarged result of the third one during the time slot 4–11.5 s. From the figure, we can see that TV1 performs VT maneuvers and stays in lane 2 almost all the time with

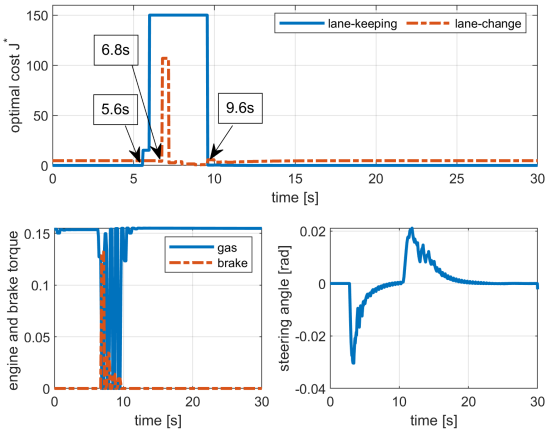

Fig. 7. Optimal cost J^* of SCMPC in two control modes and adopted control actions for Case 1.

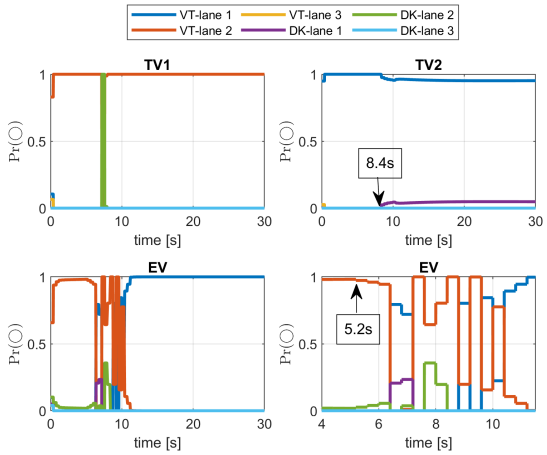

Fig. 8. Policy mode probabilities of all vehicles for Case 1. Policy mode ◯ ∈ {VT-lane 1, VT-lane 2, VT-lane 3, DK-lane 1, DK-lane 2, DK-lane 3}.

the highest probability. The tracked velocity is time-varying according to TV1's actual motion behavior.

For the EV, the VT in lane 2 mode probability increases to almost 1 from the initial setting after 0.4 s. Then, TV1, as the LV, decelerates between 2 and 5 s. Their relative distance decreases continuously. Therefore, the probability of the VT in lane 2 mode decreases at 5.2 s, while the probability of the DK in lane 2 mode increases. In addition, based on the cost of the SCMPC in two control modes, the EV initiates a lane change at 5.6 s. After analyzing the relevant innovation residual $\bar{y}_k^{(i)}$ of these two most probable modes, we conclude that their related probabilities are sometimes modified from the MIQP during simulation. For instance, at 6 s, the calculated six policy modes' state estimation errors between $\hat{z}_k^-$ and $\hat{z}_k^{(\mathrm{proj})-}$ from solving the MIQP problem are $[0.001\ 0.56\ 0.001\ 0.001\ 0.12\ 0.001]^\top$. 0.001 is a designed value representing the related state estimation error 0. The augmented estimation errors of driving in lane 2 in VT mode and DK mode, 0.56 and 0.12, decrease the corresponding modified probability in the IMM-KF. However, they are still the most likely ones. Solving the MIQP problem reduces the related probability of the mode that might lead to a collision, making the generated scenarios more reliable. During 6.4–7.2 s, the most likely mode is VT in lane 1, with a probability above 0.7, and the mode of DK in lane 1 has the

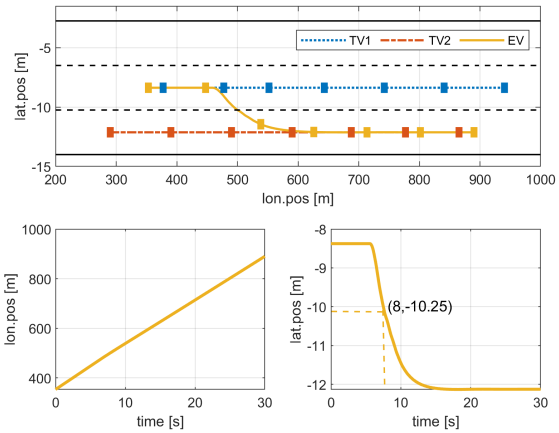

Fig. 9. Motion trajectories of all vehicles and the longitudinal and lateral positions of the EV when TV2 is aggressive.

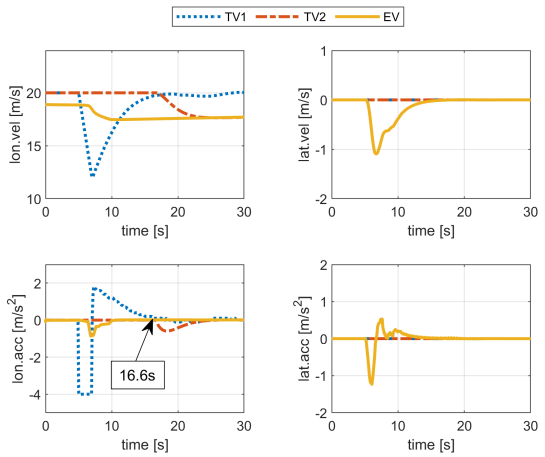

Fig. 10. Longitudinal and lateral velocities of all vehicles when TV2 is aggressive.

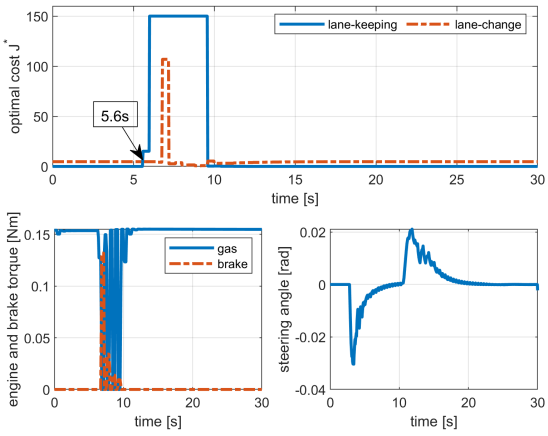

Fig. 11. Optimal cost J^* of SCMPC in two control modes and adopted control actions when TV2 is aggressive.

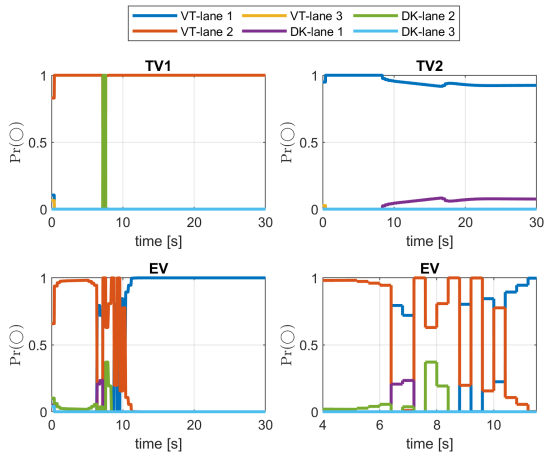

Fig. 12. Policy mode probabilities of all vehicles when TV2 is aggressive. Policy mode $\bigcirc \in$ {VT-lane 1, VT-lane 2, VT-lane 3, DK-lane 1, DK-lane 2, DK-lane 3}.

second highest probability of about 0.3. After that, the most probable mode fluctuates between staying in lane 1 or lane 2 until 10.4 s. For example, for the situation at 8 s, where the EV has entered lane 1 (as seen in Fig. 4), driving in lane 2 has the highest probability. The lateral acceleration value at this time point is around 0. By computing these two modes' innovation residual $\bar{y}_k^i$ in the lateral direction, $\bar{y}_k^{(1)} = [-0.36\ 0.17\ 1.63]^\top$ and $\bar{y}_k^{(2)} = [-0.39\ 0.17\ 0.1]^\top$, we obtain that the lateral acceleration error of staying in lane 1, equal to 1.63, is larger than that of staying in lane 2, equal to 0.1. Consequently, the second mode has a smaller innovation residual and a higher probability. From Fig. 6, we see that during lane change from 5.6 s to 9.2 s, and before the EV reaches the center position of the new lane at around 15 s, the EV's real lateral acceleration changes accordingly. It fluctuates, especially after becoming positive based on IPG CarMaker. The fluctuation makes obtaining accurate mode probability estimation difficult. Finally, the most probable mode is VT in lane 1 constantly due to the "stable" lateral acceleration.

TV2 tracks the velocity and stays in lane 1 from the beginning to 8.4 s with probability 1. After that, since the EV comes to the front of TV2 in lane 1 at 8 s, the probability of this policy mode drops to 0.95, and the probability of keeping the distance in lane 1 increases to 0.05.

Moreover, to investigate the effect of TV characteristics on EV control, the TV2's driving style is changed to aggressive by tuning the interactive parameter in IPG Carmaker, while the remaining vehicle's initial conditions are the same.

Fig. 9 shows the related motion trajectories of vehicles. The detailed velocity and acceleration profiles are represented in Fig. 10. Combined with Fig. 11, we can conclude that the EV still starts to change lanes at 5.6 s and moves to the new lane at 8 s. Finally, Fig. 12 shows the policy mode probabilities of all vehicles during simulation. The simulation results in this case are almost identical to the simulation results when TV2 aggressiveness is low. In addition, for TV2, after the EV changes lanes, it starts to decelerate at around 16.6 s, which is later than when it is more defensive. The result comparison shows that TV2, which has a lower priority than EV, does not affect the decision-making of the EV.

C. Case 2 (EV Keeps the Lanes and Brakes)

The initial traffic scene of Case 2 is shown in Fig. 13. The motion states of TV1, TV2, and EV are $x^{(\mathrm{TV1})} = [375, 22, 0, -8.38, 0, 0]^\top$, $x^{(\mathrm{TV2})} = [330, 20, 0, -12.13, 0, 0]^\top$, and $x^{(\mathrm{EV})} = [350, 18.9, 0, -8.38, 0, 0]^\top$, respectively. The corresponding priority of the three vehicles is [TV1, EV, TV2] in descending order. After 2 s, TV1

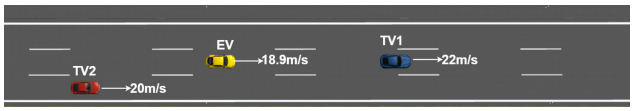

Fig. 13. Initial traffic scene for Case 2.

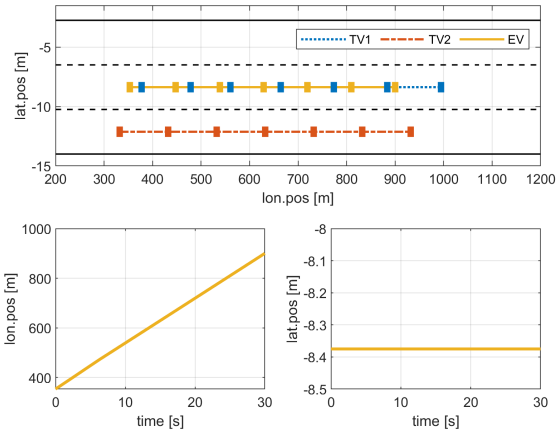

Fig. 14. Motion trajectories of all vehicles and the longitudinal and lateral positions of the EV for Case 2.

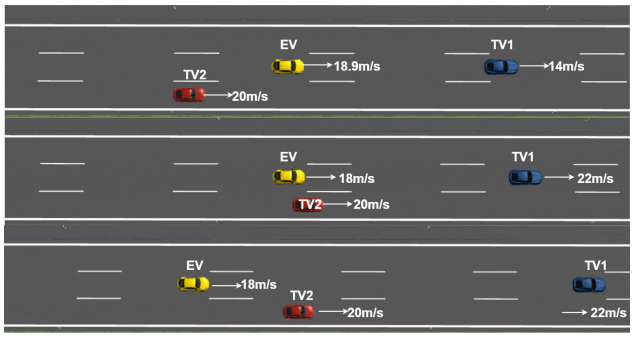

Fig. 15. Traffic scenes for Case 2 at 6, 14, and 20 s.

decelerates at -2 m/s^2 for 4 s and then accelerates back to the initial velocity of 22 m/s.

Figs. 14–17 are simulation results of Case 2. From Fig. 17, we observe that for the EV, the cost of the lane-keeping mode is always lower than that of the lane-changing mode, and it increases between 5 and 8 s. This is because TV1, as the LV of the EV, drives slower than the EV due to the deceleration between 2 and 6 s. The EV then reduces its speed to maintain the distance from TV1 until TV1 accelerates to a higher velocity than the EV. For the EV, lane change is not possible until around 16 s, as TV2 drives behind the EV with a higher speed in lane 1. Then, lane change is feasible but at a higher cost than keeping the lane. Therefore, the EV maintains its velocity in the following simulation time. TV2 drives at the initial constant speed. The vehicles' associated motion trajectories and detailed velocities are shown in Figs. 14 and 16. Fig. 15 provides some snapshots of traffic scenarios of Case 2 during simulation.

The first three subplots of Fig. 18 show the policy mode probabilities of each vehicle throughout the simulation time. The fourth subplot is a zoomed-in view of the third subplot for the time interval 5–7 s. For TV1, tracking the velocity in lane 2 is always the most likely mode with probability 1. Tracking the velocity in lane 1 is the most likely mode with probability 1 for TV2. Staying in lane 2 and tracking its velocity are the most likely mode most of the time for the EV, while between 5.6 and 6.4 s, the probability of keeping the distance mode is higher due to the deceleration of TV1.

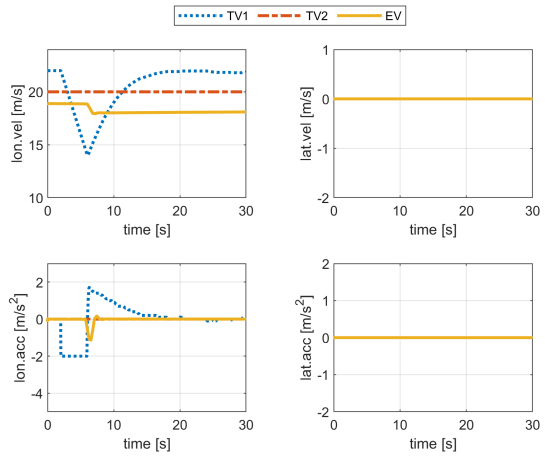

Fig. 16. Longitudinal and lateral velocities of all vehicles for Case 2.

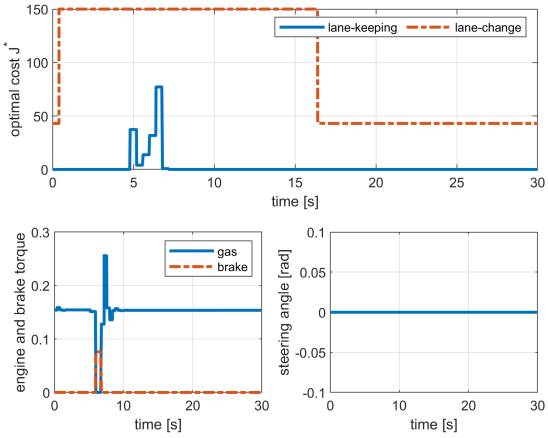

Fig. 17. Optimal cost J^* of SCMPC in two control modes and adopted control actions for Case 2.

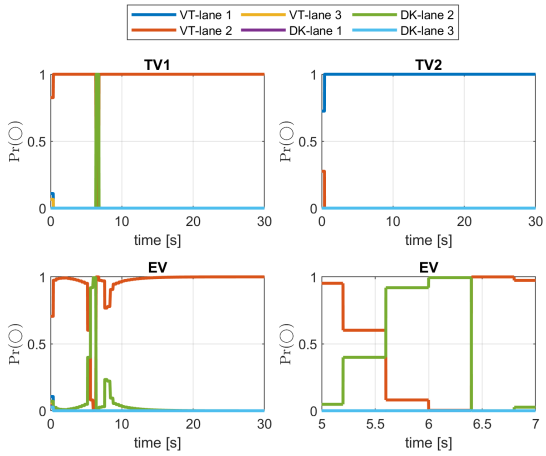

Fig. 18. Policy mode probabilities of all vehicles for Case 2. Policy mode ◯ ∈ {VT-lane 1, VT-lane 2, VT-lane 3, DK-lane 1, DK-lane 2, DK-lane 3}.

D. Case 3 (EV Changes Lanes and Keeps Velocity)

Fig. 19 shows the initial traffic scene of Case 3. Vehicles' motion states are $x^{(\mathrm{TV1})} = [375, 17, 0, -8.38, 0, 0]^\top$, $x^{(\mathrm{TV2})} = [358, 20, 0, -12.13, 0, 0]^\top$, and $x^{(\mathrm{EV})} = [350, 18.9, 0, -8.38, 0, 0]^\top$. Given the initial traffic situation,

Fig. 19. Initial traffic scene for Case 3.

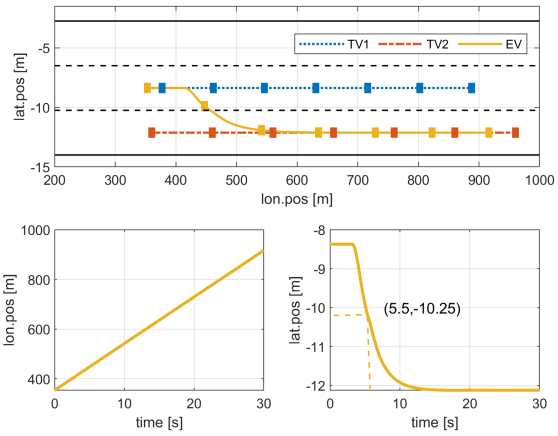

Fig. 20. Motion trajectories of all vehicles and the longitudinal and lateral positions of the EV for Case 3.

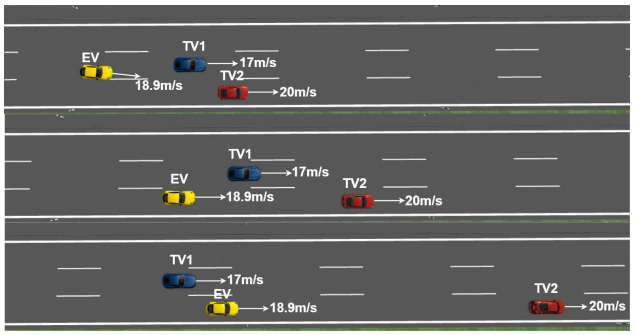

Fig. 21. Traffic scenes for Case 3 at 5, 11.5, and 26 s.

TV1 and TV2 move constantly in autonomous driving mode. The priority of the three vehicles is [TV2, TV1, EV] in descending order. The EV responds to the motion maneuvers of TV1 and TV2.

Figs. 20–23 are simulation results of Case 3. From Fig. 23, we see that even though TV1 is slower than the EV, before 3.2 s, the cost of the SCMPC in lane-keeping mode is lower than that of SCMPC in lane-changing mode. After that, as the relative distance between EV and TV1 decreases, the less costly mode switches to lane-changing mode until 7.2 s. The EV changes to lane 1 at around 5.5 s (as seen from Fig. 20). Then, since TV1 is laterally close to the EV, the EV can only stay in the new lane at a lower cost. The EV's lane-keeping and lane-changing motion behavior can be seen in Fig. 20. The EV maintains its speed throughout the simulation time.

Fig. 24 shows three vehicles' policy mode probabilities. Specifically, TV1 continually tracks the speed at 17 m/s and stays in lane 2 with a probability of around 1. TV2 maintains the initial speed and stays in lane 1 with the probability 1. As for the EV, before 4 s, it might perform VT or DK maneuvers in lane 2 with probability 0.93 and 0.07. After that, the most probable policy mode is time-varying between staying in lanes 1 and 2 until 8 s, as seen from the fourth subplot. Based on these two policy modes and the

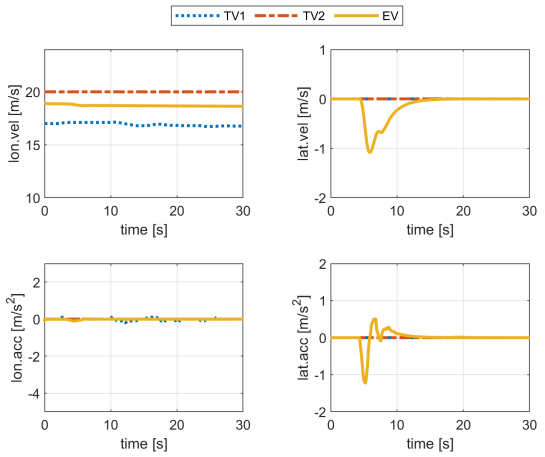

Fig. 22. Longitudinal and lateral velocities of all vehicles for Case 3.

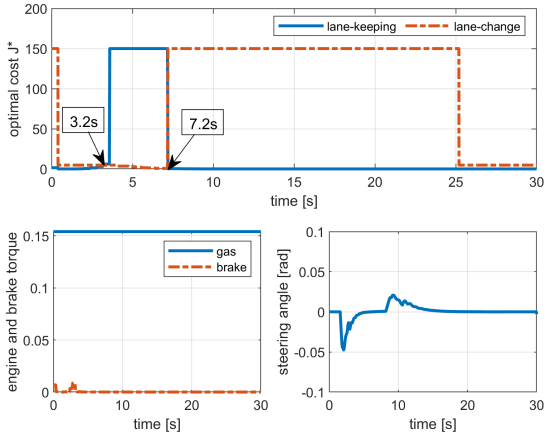

Fig. 23. Optimal cost J^* of SCMPC in two control modes and adopted control actions for Case 3.

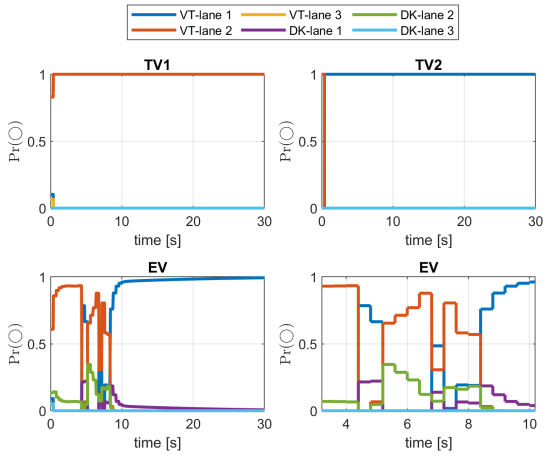

Fig. 24. Policy mode probabilities of all vehicles for Case 3. Policy mode ◯ ∈ {VT-lane 1, VT-lane 2, VT-lane 3, DK-lane 1, DK-lane 2, DK-lane 3}.

real measurements from IPG CarMaker, it is difficult for the IMM-KF to get an accurate mode probability estimation of the EV's lane change maneuver. Finally, it is most probable that the EV keeps the velocity and stays in lane 1.

VII. Conclusion and Future Work

In this article, the interaction-aware estimation of motion states of the vehicles has been studied using the IMM-KF-related approach, and the associated state predictions have

been combined with the probability to represent the uncertain environment. The IMM-KF-related method based on the MIQP reduces the probability of modes that, possibly lead to a collision, making the generated scenarios more reasonable. The generated scenarios, along with the "worst case" scenario, have been applied to formulate the safety constraints of the SCMPC. The control system consists of lane-keeping and lane-changing control modes, where the control input with a lower cost function value is implemented. Moreover, the recursive feasibility of the method has been guaranteed based on the no-collision between the EV and its LV over the minimal stopping horizon of the EV. The proposed algorithm has been validated in three highway scenarios in IPG CarMaker. The simulation results demonstrate the capability of the proposed control architecture to perform safe maneuvers. At the same time, evaluating the designed control architecture from different perspectives, such as its real-time capability, robustness, and advantages over other approaches, will be addressed in the future.

ACKNOWLEDGMENT

The authors would like to thank IPG Automotive GmbH for the Software License. They would also like to thank Dr. HaoWei Wen for participating in the discussion and providing insightful suggestions.

REFERENCES

[1] C. Gkartzonikas and K. Gkritza, "What have we learned? A review of stated preference and choice studies on autonomous vehicles," *Transp. Res. C, Emerg. Technol.*, vol. 98, pp. 323–337, Jan. 2019.

[2] M. Brannstrom, E. Coelingh, and J. Sjoberg, "Model-based threat assessment for avoiding arbitrary vehicle collisions," *IEEE Trans. Intell. Transp. Syst.*, vol. 11, no. 3, pp. 658–669, Sep. 2010.

[3] G. S. Aoude, V. R. Desaraju, L. H. Stephens, and J. P. How, "Driver behavior classification at intersections and validation on large naturalistic data set," *IEEE Trans. Intell. Transp. Syst.*, vol. 13, no. 2, pp. 724–736, Jun. 2012.

[4] S. Lefèvre, D. Vasquez, and C. Laugier, "A survey on motion prediction and risk assessment for intelligent vehicles," *ROBOMECH J.*, vol. 1, no. 1, pp. 1–14, Dec. 2014.

[5] D. Onken, L. Nurbekyan, X. Li, S. W. Fung, S. Osher, and L. Ruthotto, "A neural network approach for high-dimensional optimal control applied to multiagent path finding," *IEEE Trans. Control Syst. Technol.*, vol. 31, no. 1, pp. 235–251, Jan. 2023.

[6] J. Wang, Y. Zheng, K. Li, and Q. Xu, "DeeP-LCC: Data-enabled predictive leading cruise control in mixed traffic flow," *IEEE Trans. Control Syst. Technol.*, vol. 31, no. 6, pp. 1–17, Nov. 2023.

[7] A. Lawitzky, D. Althoff, C. F. Passenberg, G. Tanzmeister, D. Wollherr, and M. Buss, "Interactive scene prediction for automotive applications," in *Proc. IEEE Intell. Vehicles Symp. (IV)*, Jun. 2013, pp. 1028–1033.

[8] G. Agamennoni, J. I. Nieto, and E. M. Nebot, "A Bayesian approach for driving behavior inference," in *Proc. IEEE Intell. Vehicles Symp. (IV)*, Jun. 2011, pp. 595–600.

[9] V. Lefkopoulos, M. Menner, A. Domahidi, and M. N. Zeilinger, "Interaction-aware motion prediction for autonomous driving: A multiple model Kalman filtering scheme," *IEEE Robot. Autom. Lett.*, vol. 6, no. 1, pp. 80–87, Jan. 2021.

[10] J. Kong, M. Pfeiffer, G. Schildbach, and F. Borrelli, "Autonomous driving using model predictive control and a kinematic bicycle vehicle model," in *Proc. Intell. Vehicles Symp.*, Seoul, South Korea, 2015, pp. 1094–1099.

[11] J. Zhou, B. Olofsson, and E. Frisk, "Interaction-aware moving target model predictive control for autonomous vehicles motion planning," in *Proc. Eur. Control Conf. (ECC)*, 2022, pp. 154–161.

[12] Y. Chen, H. Yu, J. Zhang, and D. Cao, "Lane-exchanging driving strategy for autonomous vehicle via trajectory prediction and model predictive control," *Chin. J. Mech. Eng.*, vol. 35, no. 1, p. 71, Dec. 2022.

[13] E. F. Camacho and C. B. Alba, *Model Predictive Control*. London, U.K.: Springer, 2013.

[14] G. Cesari, G. Schildbach, A. Carvalho, and F. Borrelli, "Scenario model predictive control for lane change assistance and autonomous driving on highways," *IEEE Intell. Transp. Syst. Mag.*, vol. 9, no. 3, pp. 23–35, Fall 2017.

[15] M. Bichi, G. Ripaccioli, S. Di Cairano, D. Bernardini, A. Bemporad, and I. V. Kolmanovsky, "Stochastic model predictive control with driver behavior learning for improved powertrain control," in *Proc. 49th IEEE Conf. Decis. Control (CDC)*, Dec. 2010, pp. 6077–6082.

[16] S. H. Nair, V. Govindarajan, T. Lin, Y. Wang, E. H. Tseng, and F. Borrelli, "Stochastic MPC with dual control for autonomous driving with multi-modal interaction-aware predictions," 2022, *arXiv:2208.03525*.

[17] Y. Chen, U. Rosolia, C. Fan, A. Ames, and R. Murray, "Reactive motion planning with probabilisticsafety guarantees," in *Proc. Conf. Robot Learn.*, 2021, pp. 1958–1970.

[18] Y. Chen, U. Rosolia, W. Ubellacker, N. Csomay-Shanklin, and A. D. Ames, "Interactive multi-modal motion planning with branch model predictive control," *IEEE Robot. Autom. Lett.*, vol. 7, no. 2, pp. 5365–5372, Apr. 2022.

[19] B. Ivanovic, A. Elhafsi, G. Rosman, A. Gaidon, and M. Pavone, "MATS: An interpretable trajectory forecasting representation for planning and control," 2020, *arXiv:2009.07517*.

[20] T. A. Dingus et al., "The 100-car naturalistic driving study, phase ii-results of the 100-car field experiment," Dept. of Transportation, Nat. Highway Traffic Saf. Admin., Washington, DC, USA, Rep. DOT HS 810 593, 2006.

[21] M. A. Perez et al., "Performance of basic kinematic thresholds in the identification of crash and near-crash events within naturalistic driving data," *Accident Anal. Prevention*, vol. 103, pp. 10–19, Jun. 2017.

[22] Y. He et al., "Adaptive cruise control strategies implemented on experimental vehicles: A review," *IFAC-PapersOnLine*, vol. 52, no. 5, pp. 21–27, 2019.

[23] S. Magdici and M. Althoff, "Adaptive cruise control with safety guarantees for autonomous vehicles," *IFAC-PapersOnLine*, vol. 50, no. 1, pp. 5774–5781, Jul. 2017.

[24] S. Shalev-Shwartz, S. Shammah, and A. Shashua, "On a formal model of safe and scalable self-driving cars," 2017, *arXiv:1708.06374*.

[25] X. Xu, X. Wang, X. Wu, O. Hassanin, and C. Chai, "Calibration and evaluation of the responsibility-sensitive safety model of autonomous car-following maneuvers using naturalistic driving study data," *Transp. Res. C, Emerg. Technol.*, vol. 123, Feb. 2021, Art. no. 102988.

[26] X. Zhang, S. Zeinali, and G. Schildbach, "Interaction-aware traffic prediction and scenario-based model predictive control for autonomous vehicles on highways," in *Proc. Eur. Control Conf. (ECC)*, Jun. 2024, pp. 3351–3357.

[27] R. Schmied, H. Waschl, and L. del Re, "Extension and experimental validation of fuel efficient predictive adaptive cruise control," in *Proc. Amer. Control Conf. (ACC)*, Jul. 2015, pp. 4753–4758.